


Article

Renewable Butene Production through Dehydration Reactions over Nano-HZSM-5/ γ -Al₂O₃ Hybrid Catalysts

Arno de Reviere ^{1,2,†} , Tom Vandevyvere ^{1,2,†}, Maarten K. Sabbe ^{1,2} and An Verberckmoes ^{1,*}

¹ Industrial Catalysis and Adsorption Technology (INCAT), Department of Materials, Textiles and Chemical Engineering (MaTCh), Faculty of Engineering and Architecture, Ghent University, Valentin Vaerwyckweg 1, 9000 Ghent, Belgium; Arno.deReviere@ugent.be (A.d.R.); Tom.Vandevyvere@ugent.be (T.V.); Maarten.Sabbe@ugent.be (M.K.S.)

² Laboratory for Chemical Technology (LCT), Department of Materials, Textiles and Chemical Engineering (MaTCh), Faculty of Engineering and Architecture, Ghent University, Technologiepark 125, 9052 Ghent, Belgium

* Correspondence: An.Verberckmoes@ugent.be

† These authors contributed equally to this work.

Received: 15 July 2020; Accepted: 31 July 2020; Published: 4 August 2020



Abstract: The development of new, improved zeolitic materials is of prime importance to progress heterogeneous catalysis and adsorption technologies. The zeolite HZSM-5 and metal oxide γ -Al₂O₃ are key materials for processing bio-alcohols, but both have some limitations, i.e., HZSM-5 has a high activity but low catalytic stability, and vice versa for γ -Al₂O₃. To combine their advantages and suppress their disadvantages, this study reports the synthesis, characterization, and catalytic results of a hybrid nano-HZSM-5/ γ -Al₂O₃ catalyst for the dehydration of n-butanol to butenes. The hybrid catalyst is prepared by the in-situ hydrothermal synthesis of nano-HZSM-5 onto γ -Al₂O₃. This catalyst combines mesoporosity, related to the γ -Al₂O₃ support, and microporosity due to the nano-HZSM-5 crystals dispersed on the γ -Al₂O₃. HZSM-5 and γ -Al₂O₃ being in one hybrid catalyst leads to a different acid strength distribution and outperforms both single materials as it shows increased activity (compared to γ -Al₂O₃) and a high selectivity to olefins, even at low conversion and a higher stability (compared to HZSM-5). The hybrid catalyst also outperforms a physical mixture of nano-HZSM-5 and γ -Al₂O₃, indicating a truly synergistic effect in the hybrid catalyst.

Keywords: hybrid catalyst; nano-HZSM-5/ γ -Al₂O₃; alcohol dehydration; nano-HZSM-5; γ -Al₂O₃; bio-based butenes

1. Introduction

Due to increasing environmental awareness, there has been a shift toward bio-based products and the design of sustainable, renewable technologies [1–3]. In light of a transition to a more sustainable chemical industry, there has been a lot of interest in the production and use of bio-alcohols [4,5]. Bio-alcohols can be used as additives to fuels [6,7], as solvents, or even as feedstock for chemical processing [8,9]. Alcohols can undergo dehydration to olefins, which are of the most extensively used building blocks in the chemical industry [10,11].

Zeolites and γ -Al₂O₃ could play a key role in the transition from a fossil-based industry into a renewable industry as they are of the most important materials used in traditional oil processing and heterogeneous catalysis [12–15]. Zeolites, and, more specifically, HZSM-5, are essential materials in mature technologies such as fluid catalytic cracking (FCC) [16,17] and alkylation reactions [18,19], but also in more recent technologies such as methanol-to-olefins (MTO) [20,21]. HZSM-5 is known for its shape selectivity, strong intrinsic acidity [19], and thermal stability, but is also prone to coking [22,23].

Alumina materials, on the other hand, are of the most important catalyst supports, for example, γ -Al₂O₃ is used in reforming reactions [24], hydrotreating, and hydroconversion [25–27]. Alumina materials are widely used due to their low cost, thermal stability, fairly high surface area, and pore volume [25,28,29].

To convert alcohols, e.g., ethanol or butanol, to olefins, two catalysts, (i) HZSM-5 and (ii) γ -Al₂O₃, are the most investigated materials [30–35], and are already used at an industrial scale for ethanol dehydration [32,36]. Although HZSM-5 and γ -Al₂O₃ are extensively used, they have their limits. For the dehydration of bio-alcohols, HZSM-5 typically has a very high activity and selectivity to the corresponding olefins; however, the stability is poor due to coking [37]. Furthermore, beyond full conversion, secondary reactions are also catalyzed [38]. For γ -Al₂O₃, it is the opposite: It has a low activity, requiring higher temperatures; moreover, a high selectivity toward olefins also requires sufficiently high temperatures [32]. On the other hand, the catalyst has a high stability under dehydration reaction conditions. Their performance is somewhat the opposite and can be related to their very different properties, summarized in Table 1.

Table 1. Characteristic properties of HZSM-5 and γ -Al₂O₃ [39,40].

Material	Porosity	Acid Type	Acid Strength	Crystallinity
HZSM-5	microporous	mostly Brønsted	strong	high
γ -Al ₂ O ₃	mesoporous	Lewis	medium	low to semi

To avoid these shortcomings, there have been studies on modifying these catalysts. Decreasing the HZSM-5 crystal size to nanocrystals has shown an increase in the catalyst life time [41] and is often associated with an increase in activity [42]. This increase in stability and activity is often related to the decrease in diffusion pathlength inside the micropores and/or lowered deactivation due to coking. Other strategies include inducing mesoporosity [43] and modification of the acid sites by post-synthesis treatments [44], e.g., phosphorus-modifications decrease the strength of the acid sites and thereby attenuate coke formation [45]. Instead of creating mesopores inside the zeolite particle, it is also possible to synthesize the zeolite on a mesoporous material (such as MCM-41) [46]: This can enhance the performance by suppressing zeolite crystal aggregation, inducing dilution of the zeolitic Brønsted acid centers, and creating mesoporosity, which leads to a lower acid density and can attenuate diffusional restrictions [47,48].

For γ -Al₂O₃, the modifications typically aim to increase the activity and allow lower reaction temperatures [32]. By modifying the γ -Al₂O₃ with TiO₂, the acidity increased, resulting in a higher activity. Modification of the γ -Al₂O₃ surface with Zn-Mn-Co increases the acid strength and crystallinity, which results in an increased activity [49,50].

He et al. found that the combination of γ -Al₂O₃ and HZSM-5 into one catalyst leads to an increased selectivity toward light olefins for the pyrolysis of waste tires [51]. Due to their interesting findings, and the fact that HZSM-5 and γ -Al₂O₃ are two widely used catalytically active materials for the dehydration of alcohols, the objective of this work is to develop a hybrid catalyst that is a combination of HZSM-5 and γ -Al₂O₃. The combination is aimed to be in such a manner that the advantages of both catalysts are combined, namely (i) a high activity and selectivity to olefins related to HZSM-5 nanocrystals, i.e., no high temperatures are needed for bio-alcohol dehydration, and (ii) a strong resistance to deactivation related to the presence of γ -Al₂O₃. To achieve these synergistic effects, the nano-HZSM-5 is synthesized upon γ -Al₂O₃, which acts as a catalytically active support and leads to mesopores with mildly active sites in the vicinity of the active sites of HZSM-5. To this end, a hybrid catalyst, composed of in-situ-synthesized nano-HZSM-5 crystals dispersed on a γ -Al₂O₃ active support, was manufactured. To the best of our knowledge, this is the first report where the synergistic effects of combining both catalysts in one hybrid material is exploited for the dehydration of bio-alcohols to olefins. The dehydration of n-butanol at 513 K is used as a test reaction to compare

the hybrid catalyst to HZSM-5, γ -Al₂O₃, and a physical mixture of both. The catalytic performance (activity/selectivity/stability) is then related to the properties of the studied materials.

2. Results and Discussion

2.1. Catalyst Characterization

The XRD patterns of the commercially available HZSM-5 (c-HZSM-5), the synthesized nano-HZSM-5 (n-HZSM-5), the physical mixture of nano-HZSM-5 and γ -Al₂O₃ (PM-50/50), the hybrid catalyst (Hybrid-50/50), and commercially available γ -Al₂O₃ are presented in Figure 1.

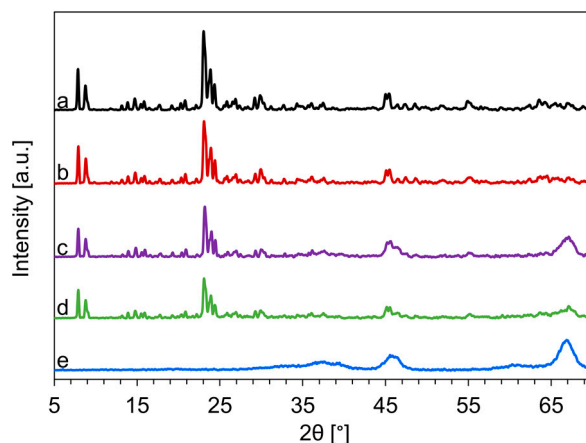


Figure 1. XRD-pattern of commercially available (c)-HZSM-5 (a), nano (n)-HZSM-5 (b), physical mixture of nano-HZSM-5 and γ -Al₂O₃ (PM-50/50) (c), the hybrid catalyst (Hybrid-50/50) (d), and γ -Al₂O₃ (e).

The diffraction patterns between 7.5 and 9° and between 22.5° and 26° are attributed to the ZSM-5 structure. The intensity in these ranges of 2 θ is the highest for c-HZSM-5 and n-HZSM-5, which is as expected as these are pure zeolite phases, while PM-50/50 and Hybrid-50/50 are mixtures of zeolite phases and γ -Al₂O₃. Albeit a lower intensity, the diffraction pattern at these angles is identical, which indicates that the Hybrid-50/50 synthesis is successful and the ZSM-5 crystals can be synthesized alongside γ -Al₂O₃. The peaks related to the HZSM-5 phase are for all catalysts sharp, and have a high intensity, which is typical for highly crystalline HZSM-5 [52]. In the pattern of PM-50/50 and Hybrid-50/50, broader diffraction peaks due to the γ -Al₂O₃ phases are also present, indicating that both catalysts consist of both HZSM-5 and γ -Al₂O₃. The mean HZSM-5 crystal size determined by the Scherrer equation, Equation (1), is 160 nm for c-HZSM-5, 118 nm for n-HZSM-5, and 114 nm for Hybrid-50/50. As the HZSM-5 particles in PM-50/50 are the n-HZSM-5 ones, their mean crystal size should also be 118 nm.

N₂-sorption isotherms of the various materials are displayed in Figure 2. From the isotherms, it is clear that c-HZSM-5 and n-HZSM-5 are highly microporous and show a type Ia isotherm according to the Brunauer–Deming–Deming–Teller classification. This type of isotherm corresponds to microporous solids with narrow micropores (width < 1 nm) [8]. Where n-HZSM-5 is almost completely microporous, there is some mesoporosity in c-HZSM-5 noticeable. The isotherm of c-HZSM-5 has a hysteresis of type H4, which can be ascribed to the capillary condensation of N₂ in interparticles or in crystal agglomerates [53]. The γ -Al₂O₃, PM-50/50, and Hybrid-50/50 clearly display strong mesoporosity, although there is also microporosity noticeable in the latter two due to the presence of HZSM-5 crystals. The isotherm of γ -Al₂O₃ is of type IV, while for PM-50/50 and Hybrid-50/50, the isotherm starts off as a type I but evolves into a type IV.

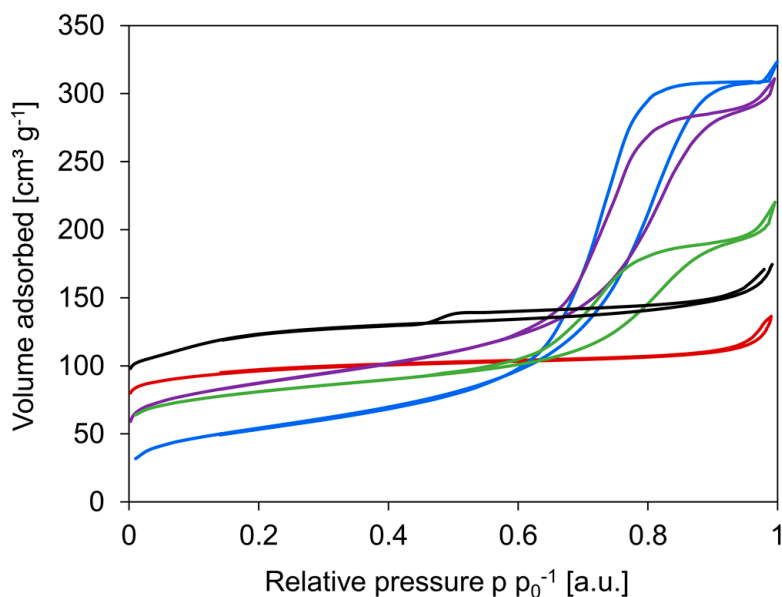


Figure 2. Nitrogen sorption isotherms for c-HZSM-5 (black), n-HZSM-5 (red), γ -Al₂O₃ (blue), PM-50/50 (purple), and Hybrid-50/50 (green).

From these isotherms, it is possible to gain insights into how the synthesis of the catalysts influences their textural properties: Specific surface area, specific pore volume, and pore size distribution analysis are performed (see Figure 3 and Table 2). The specific surface area of c-HZSM-5 is the highest, followed by n-HZSM-5. PM-50/50 and Hybrid-50/50 have intermediate surface areas, whereas γ -Al₂O₃ has the lowest surface area. The obtained pore sizes of c-HZSM-5 and n-HZSM-5 (Figure 3a) show good agreement with the pore diameter of approximately 0.5 nm for the MFI framework. Furthermore, there are some small mesopores measured (d_p about 2–2.5 nm). Analyzing the pore structures (Figure 3b) shows that the mesopore volume is largest for γ -Al₂O₃. The mesoporosity measured for PM-50/50 is attributed to the γ -Al₂O₃, which is present in the mixture, and the pore dimensions of the mesopores are unaltered for PM-50/50, although the mesopore volume has dropped as expected. For the Hybrid-50/50, a much stronger decrease in mesopore volume is noticeable, although the pore diameter of the mesopores is unaltered, meaning that, most likely, there are no HZSM-5 crystals inside the mesopores of the γ -Al₂O₃ support, but they are instead formed on the external surface.

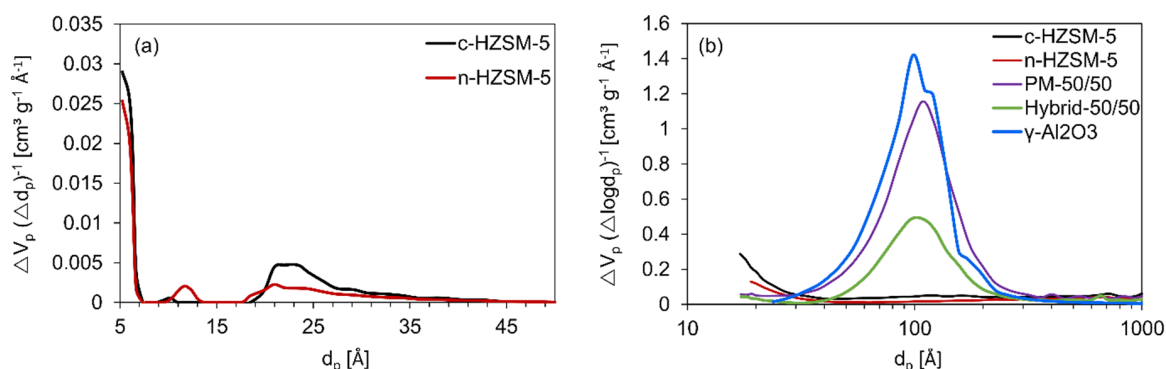


Figure 3. Non-local density functional theory (NLDFT) pore size distribution of c-HZSM-5 and n-HZSM-5 (a), and Barrett, Joyner, and Halenda (BJH) pore size distribution of the catalysts studied in this work (b).

Table 2. Textural properties of the catalysts used in this work.

Catalyst	S _{BET} (m ² g ⁻¹)	S _{micro} (m ² g ⁻¹)	S _{meso} (m ² g ⁻¹) ^a	V _{micro} (cm ³ g ⁻¹)	V _t (cm ³ g ⁻¹)
c-HZSM-5	410	230	180	0.11	0.24
n-HZSM-5	370	280	90	0.11	0.16
PM-50/50	310	130	180	0.063	0.45
Hybrid-50/50	303	172	131	0.084	0.26
γ-Al ₂ O ₃	195	2	193	0.00	0.49

$$^a S_{\text{meso}} = S_{\text{BET}} - S_{\text{micro}}$$

The results extracted from the NH₃-TPD are summarized in Table 3. The spectra at a ramp rate of 10 K min⁻¹ are shown in Figures S2 and S3. From these results, it is clear that the Hybrid-50/50 catalyst, its density of strong acid sites, and its total amount of acid sites are substantially lower than those for the other catalysts. This can be partially explained by the synthesis method: During the synthesis, the γ-Al₂O₃ is added to the zeolite precursor mixture, which is at a pH of about 12. The hydroxyl groups (originating from tetrapropylammonium hydroxide (TPAOH)) in this mixture can interact with the acid sites on the γ-Al₂O₃ and even partially dissolve the alumina [54], thereby decreasing the number of acid sites. Furthermore, the HZSM-5 crystals being on the γ-Al₂O₃ surface can block some of the previously available acid sites. Not only has the amount of acid sites changed, but so has the distribution of the acid strength, where n-HZSM-5 and γ-Al₂O₃ primarily have “strong” acid sites, and the Hybrid-50/50 has more “medium” acidic active sites than “strongly” acidic. Based on the NH₃-desorption energy, the NH₃ is adsorbed the strongest on n-HZSM-5 and the weakest on γ-Al₂O₃. Both PM-50/50 and Hybrid-50/50 have intermediate NH₃-desorption energies, although for Hybrid-50/50, which consists of nano-HZSM-5 crystals and γ-Al₂O₃, the E_d is almost the same as for c-HZSM-5.

Table 3. NH₃-TPD results for the catalysts used in this work.

Catalyst	Amount of Acid Sites (μmol g ⁻¹)				E _d (kJ mol ⁻¹) ^a
	Weak	Medium	Strong	Total	
c-HZSM-5	156	68	199	422	130
n-HZSM-5	118	83	193	394	150
PM-50/50	154	70	152	376	115
Hybrid-50/50	129	94	50	273	128
γ-Al ₂ O ₃	137	123	190	450	92

^a Calculated for the highest-temperature peak, based on Equation (2).

Through SEM, the morphological details of the catalysts are studied, Figure 4, and further magnified images are shown in Figure S4. The c-HZSM-5 has irregularly shaped, aggregated crystals, confirming the possibility of intercrystalline mesoporosity, which was deduced from N₂-sorption. The crystal size ranges from about 80 to 600 nm. The n-HZSM-5 has far more regularly hexagonal or coffin-shaped nanocrystals (see Figure S4) and a much smaller range of crystal sizes (about 80–180 nm). For PM-50/50, both separate n-HZSM-5 and γ-Al₂O₃ phases are noticeable. From the SEM images, no interaction between both phases is observable. For the Hybrid-50/50, on the other hand, it is clearly noticeable that the n-HZSM-5 crystals are dispersed on the surface of the γ-Al₂O₃, rather than having two separate phases. Therefore, it seems likely that the in-situ synthesis of HZSM-5 in the presence of γ-Al₂O₃ leads to an interaction between the HZSM-5 nanocrystals and the γ-Al₂O₃ support. The γ-Al₂O₃ particles are regularly shaped spheres with a diameter between 100 and 150 μm.

2.2. Catalytic Performance for the Dehydration of n-Butanol

2.2.1. Activity Analysis

To compare the activity of the catalysts, the n-butanol dehydration was performed at a single temperature of 513 K, as γ-Al₂O₃ and HZSM-5 display some activity for the dehydration of n-butanol at

this temperature [38], see Figure 5. For the dehydration of n-butanol, the order of activity is c-HZSM-5 > n-HZSM-5 > Hybrid-50/50 > PM-50/50 >> γ -Al₂O₃.

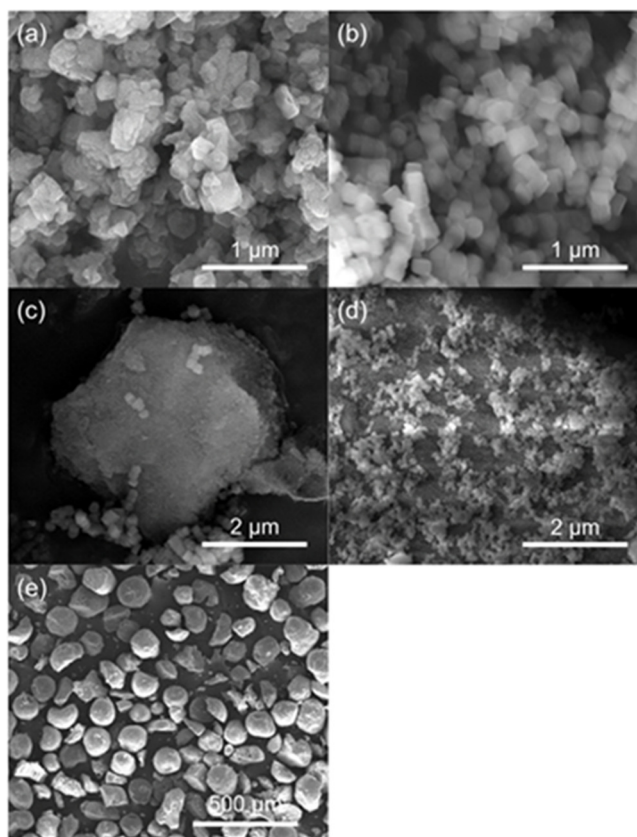


Figure 4. SEM images of c-HZSM-5 (a), n-HZSM-5 (b), PM-50/50 (c), Hybrid-50/50 (d), and γ -Al₂O₃ (e).

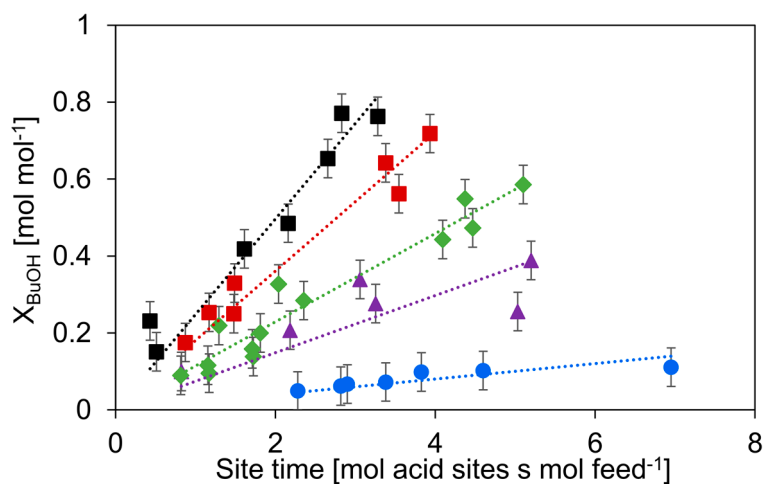


Figure 5. Conversion of n-butanol versus site time for c-HZSM-5 (■, black), n-HZSM-5 (■, red), PM-50/50 (▲, purple), Hybrid-50/50 (◆, green), and γ -Al₂O₃ (●, blue). Temperature = 513 K, inlet pressure of n-butanol = 29 kPa, total pressure = 5 bar. Error bars indicate the 95% confidence interval.

As expected, the c-HZSM-5 and n-HZSM-5 show the highest activity, most likely related to their strong acidity and relatively small pore sizes, which increases the interaction with the reactant [55]. The slightly higher activity of c-HZSM-5 compared to n-HZSM-5 can be attributed to the high ratio of strong acid sites over medium acid sites. The activity, expressed as site time yield (STY, defined in Equation (5), comprising both medium and strong acid sites) is linearly related to this ratio for every

catalyst except for Hybrid-50/50 (see Figure 6), showing that the catalyst is acting non-linear compared to its constituents.

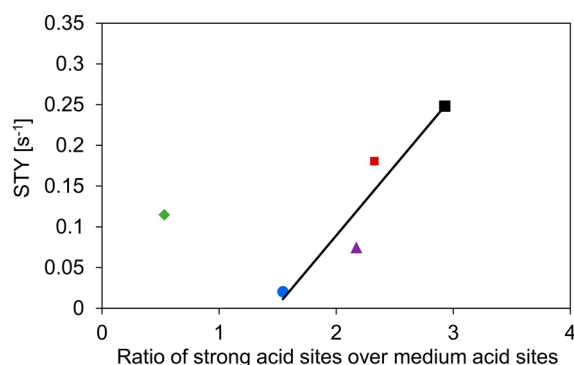


Figure 6. Site time yield (STY) as a function of the ratio of the amount of strong acid sites over medium acid sites. Symbols: c-HZSM-5 (■, black), n-HZSM-5 (■, red), PM-50/50 (▲, purple), Hybrid-50/50 (◆, green), and γ -Al₂O₃ (●, blue). Temperature = 513 K, inlet pressure of n-butanol = 29 kPa, total pressure = 5 bar.

As can be seen in Figure 6, the activity generally increases linearly with increasing ratio of the densities of the strong acid sites over medium acid sites. The only catalyst strongly deviating from this trend is Hybrid-50/50. We expect that this is due to a synergistic interaction between γ -Al₂O₃ and the nano-HZSM-5 crystals in the hybrid catalyst. Furthermore, the nano-HZSM-5 crystals being dispersed on the alumina surface increases the accessibility of the zeolitic or Brønsted acid sites, leading to a possibly more efficient active site. Furthermore, Wang et al. found that if there are Lewis acid sites introduced in the vicinity of Brønsted acid sites in HZSM-5, the dehydration of ethanol is facilitated [56]. Although the acid sites of Hybrid-50/50 are more active than what would be expected, they are still less active than HZSM-5.

The Hybrid-50/50 has a higher activity than PM-50/50, which could be related to the interaction between the nano-HZSM-5 crystals and the γ -Al₂O₃ support, which leads to a more efficient conversion of the alcohol. The high activity of Hybrid-50/50 and PM-50/50 compared to γ -Al₂O₃ is related to the presence of HZSM-5 nanocrystals. Another aspect that influences the catalyst activity is the reaction pathways that are followed. In the work of Gunst et al. it was shown that a stable dibutyl ether surface species can occupy over 95% of the available acid sites in HZSM-5 during the dehydration of n-butanol [31]. The high surface coverage by dibutyl ether decreases the activity as the alternative reaction pathways (e.g., direct dehydration from n-butanol to 1-butene) are suppressed. In our previous work, we showed that dibutyl ether is the main product over γ -Al₂O₃ below conversions of 0.6 mol mol⁻¹ [38]. This can implicate that if the γ -Al₂O₃ significantly contributes during the dehydration reaction and mainly forms dibutyl ether, the activity of the nano-HZSM-5 is lowered because of the poisoning by dibutyl ether. To gain more insights into the behavior of Hybrid-50/50 and PM-50/50 and validate our assumption, a selectivity analysis is performed.

2.2.2. Selectivity Analysis

The selectivity toward the dehydration products of the catalysts is compared in Figure 7 (and Figure S6 with error bars). Of all studied catalysts, only γ -Al₂O₃ does not actively catalyze the isomerization of the butenes. In earlier work, it is reported that both the butenes and dibutyl ether (DBE) are primary products over HZSM-5, whilst for γ -Al₂O₃, only 1-butene and dibutyl ether are directly formed [31,38].

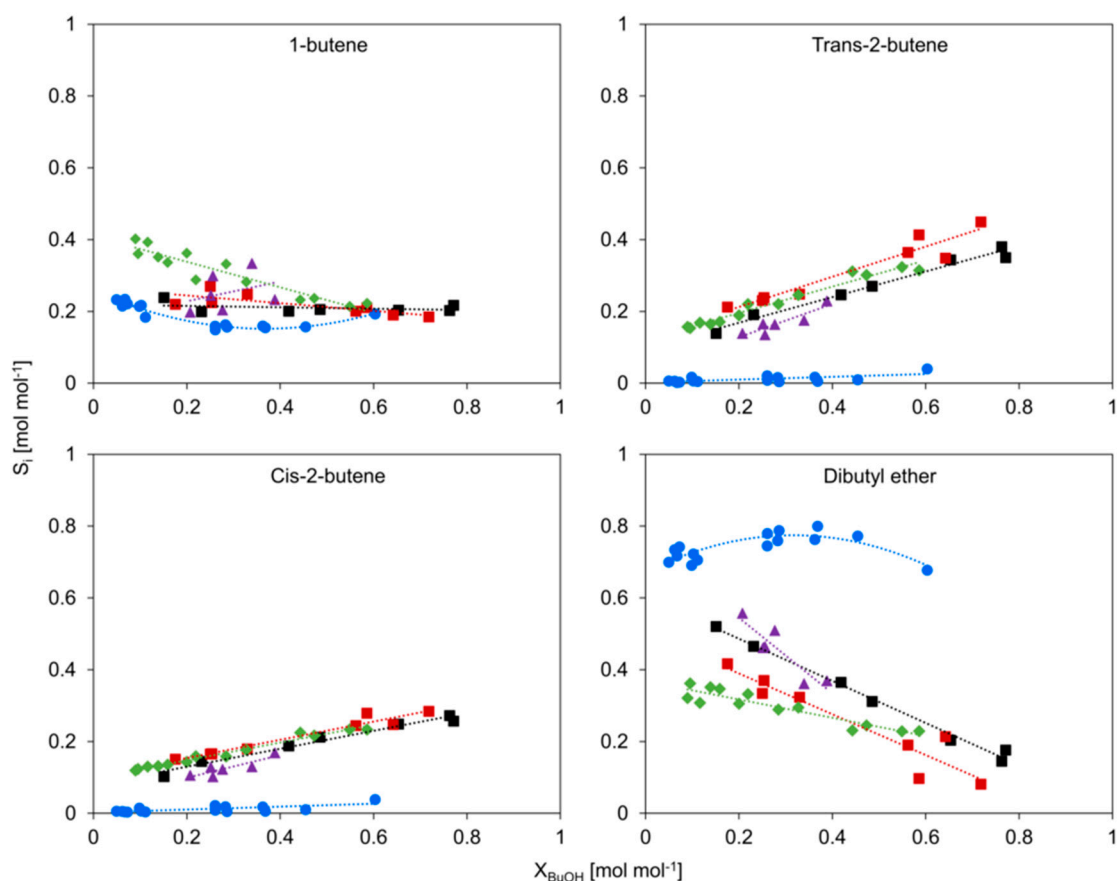


Figure 7. Selectivity of products versus conversion, c-HZSM-5 (■, black), n-HZSM-5 (■, red), PM-50/50 (▲, purple), Hybrid-50/50 (◆, green), and γ -Al₂O₃ (●, blue). Temperature = 513 K, inlet pressure of n-butanol = 29 kPa, total pressure = 5 bar.

For most catalysts, the selectivity toward 1-butene is relatively stable at approximately 0.2 mol mol⁻¹. Hybrid-50/50 starts at a slightly higher 1-butene selectivity, but with increasing conversion, it approaches a similar value as the other catalysts. The higher initial 1-butene selectivity is most likely related to (i) the presence of γ -Al₂O₃, which catalyzes the formation of 1-butene but does not catalyze the isomerization reactions of 1-butene, and (ii) because, at low conversion, the surface of the HZSM-5 crystals is saturated with adsorbed alcohol and ether [30], thereby suppressing butene isomerization reactions. At higher conversion, the partial pressure of n-butanol decreases, allowing isomerization of the butenes, leading to a lower 1-butene selectivity. For n-HZSM-5 and c-HZSM-5, the selectivity toward 1-butene is identical and corresponds well with the literature [30,31,38].

The selectivity toward cis- and trans-2-butene is very similar for all studied materials except for γ -Al₂O₃. Not only the trends in the selectivity profile but also the absolute values of the selectivity agree well for every material containing HZSM-5 crystals. The selectivity toward trans-2-butene is slightly higher for n-HZSM-5 than for c-HZSM-5 and, correspondingly, the selectivity toward dibutyl ether is slightly higher for c-HZSM-5. This is attributed to the lack of mesopores in n-HZSM-5, and the formation of the bulkier dibutyl ether preferentially occurs at the largest voids inside the zeolite. As c-HZSM-5 has some mesoporosity, it has larger voids where dibutyl ether is preferentially formed.

γ -Al₂O₃ has the highest and PM-50/50 has the second highest selectivity toward dibutyl ether, which is most likely related to the high amount of γ -Al₂O₃ present in PM-50/50. Therefore, both γ -Al₂O₃ and HZSM-5 are important contributors to the activity and selectivity over PM-50/50. On the contrary, instead of having an intermediate selectivity toward dibutyl ether, Hybrid-50/50 has the lowest selectivity to it of all studied catalysts at low conversion. With increasing conversion, the selectivity toward DBE over Hybrid-50/50 approaches the values obtained over HZSM-5. The low selectivity

toward dibutyl ether could explain why the activity of Hybrid-50/50 is higher than the activity of PM-50/50. We propose that the low selectivity of dibutyl ether over Hybrid-50/50 is related to the synthesis procedure, where the γ - Al_2O_3 is intensely mixed in the zeolite precursor solution at high pH. As mentioned in Section 2.1, we assume that during the synthesis, the basic hydroxyl groups originating from TPAOH interact with the surface of γ - Al_2O_3 and deactivate some of the strong Lewis acid sites. It is possible that the decrease in strong acid sites during synthesis is reflected in a lowered selectivity toward DBE and a shift in dominant reaction pathways to allow more butene formation, which consequently leads to a higher activity than expected.

2.2.3. Catalyst Stability

Next to activity and selectivity, stability is an important parameter to assess the catalyst performance. To this end, a deactivation study was performed, and the results are shown in Figure 8. The reaction was performed at 513 K and at site times where the conversion was similar for every catalyst.

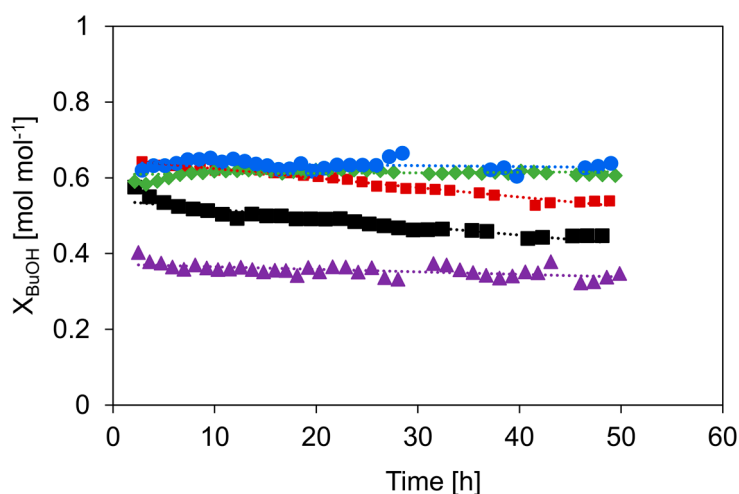


Figure 8. X_{BuOH} as a function of time on stream: c-HZSM-5 (■, black), n-HZSM-5 (■, red), PM-50/50 (▲, purple), Hybrid-50/50 (◆, green), and γ - Al_2O_3 (●, blue). Temperature = 513 K, inlet pressure of n-butanol = 29 kPa, total pressure = 5 bar.

Although all catalysts are relatively stable, the strongest deactivation over time is noticeable for c-HZSM-5, for which the conversion decreases from 0.58 to 0.45 mol mol⁻¹ in 48 h. The self-synthesized n-HZSM-5 is more resistant to deactivation: The conversion decreases from 0.64 to 0.54 mol mol⁻¹ in 48 h. Where the deactivation of c-HZSM-5 is the most severe in the first 15 h and then slows down, the n-HZSM-5 has an overall more gradual deactivation. The increased resistance to deactivation of n-HZSM-5 is most likely related to the, on average, smaller crystal size and the narrower crystal size distribution, resulting in a shorter microporous diffusion pathlength compared to c-HZSM-5. As the zeolite nanocrystals easily aggregate, there can be localized higher densities of strong acid sites prone to coke formation, and, therefore, the n-HZSM-5 can still deactivate significantly over time. On the other side of the spectrum, there is γ - Al_2O_3 , for which no measurable deactivation is observed over 48 h. This is as expected as γ - Al_2O_3 is known for its high stability under alcohol dehydration conditions [36,57].

PM-50/50 also has a slightly stronger deactivation during the first hours, but then becomes more stable. The initial deactivation is attributed to the presence of nano-HZSM-5, but over time, the catalyst keeps most of its activity due to the presence of γ - Al_2O_3 . Hybrid-50/50 seems, similar to γ - Al_2O_3 , to be very stable and shows no measurable deactivation during 48 h on stream. This is quite peculiar because, based on the relatively high activity and the observed selectivity profile, a deactivation behavior somewhere between γ - Al_2O_3 and HZSM-5 would be expected. While the deactivation behavior is very similar to that of γ - Al_2O_3 , the selectivity toward the products is very similar to that of HZSM-5

during the deactivation study (see Figure 9). This is quite remarkable as the selectivity versus time on the stream profile implies that the nano-HZSM-5 crystals of Hybrid-50/50 must be dominantly contributing during the complete run. However, there is no measurable deactivation, while there is definitely deactivation noticeable for the pure n-HZSM-5. We assume that this strong increase in resistance to deactivation for Hybrid-50/50 is related to the decrease in aggregation of the HZSM-5 nanocrystals due to the dispersion and interaction with the γ -Al₂O₃ surface. A similar observation is reported by Castaño et al. where the coke formation during the methanol-to-hydrocarbon conversion was significantly reduced by decreasing the aggregation of HZSM-5 crystals inside catalyst extrudates consisting of HZSM-5, a pseudo-boehmite binder, and α -Al₂O₃ filler [58]. Next to the decrease in crystal aggregation, the mesopores of γ -Al₂O₃ in the vicinity of the nano-HZSM-5 crystals allow more efficient transport of the products (i.e., product removal) and could avoid coke formation.

The intermediate activity of Hybrid-50/50, combined with the high selectivity toward olefins and the high stability during the conversion of bio-butanol, indicates a beneficial effect that is possibly related to the close proximity of active sites of HZSM-5 and those of γ -Al₂O₃, because of the high dispersion of the HZSM-5 nanocrystals on the γ -Al₂O₃.

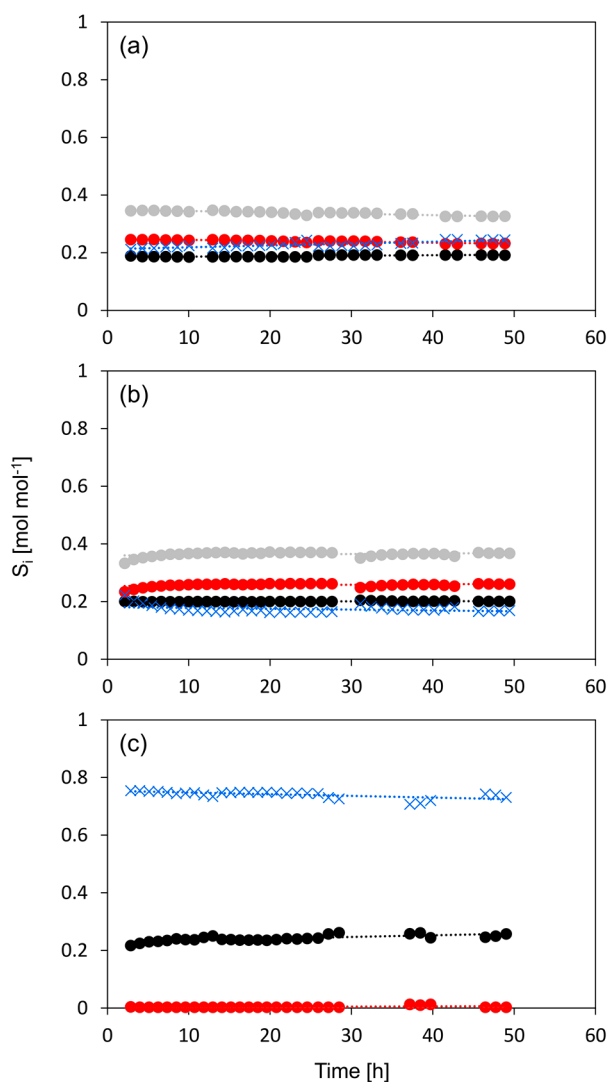


Figure 9. Selectivity to the dehydration products of n-butanol versus time on stream, for n-HZSM-5 (a) Hybrid-50/50 (b) and γ -Al₂O₃ (c). 1-butene (●, black), cis-2-butene (●, red), trans-2-butene (●, grey), dibutyl ether (×, blue). Temperature = 513 K, inlet pressure of n-butanol = 29 kPa, total pressure = 5 bar.

3. Materials and Methods

3.1. Catalyst Synthesis

In this work, both commercially available as well as self-synthesized catalysts were used: HZSM-5 (Zeolyst, CBV 5524 G, referred to as c-HZSM-5, Si/Al ratio = 25 according to the manufacturer) and γ -Al₂O₃ (Sasol, Puralox SCCa-150-200) were bought; all the other catalysts were synthesized. The self-synthesized materials were: (1) A nano-sized HZSM-5 (n-HZSM-5, aimed at a Si/Al ratio of 25), (2) a hybrid catalyst consisting of 50 mass% in-situ-synthesized nano-HZSM-5 crystals dispersed on a γ -Al₂O₃ surface (Hybrid-50/50), and (3) a physical mixture of 50 mass% nano-HZSM-5 and 50 mass% γ -Al₂O₃ (PM-50/50), for which no molecular interaction between the two phases is expected.

The synthesis of the nano-HZSM-5 material was based upon the method reported by Song et al. [59], but was slightly adjusted. First, aluminum isopropoxide ($\geq 98\%$, Merck) was dissolved in tetrapropylammonium hydroxide (TPAOH, 1 M in water, Merck) under continuous stirring to obtain a clear solution, and this was followed by addition of H₂O, then NaOH ($\geq 98\%$, Merck), and finally tetraethyl orthosilicate (TEOS, $\geq 99\%$, ChemLab) to obtain a synthesis solution, which was hydrolyzed at room temperature for 24 h. The obtained mixture was transferred into a Teflon-lined stainless-steel autoclave, where the solution underwent hydrothermal reaction at 165 °C for 96 h. The molar composition of the synthesis mixture was 1 Al/25 Si/9 TPAOH/495 H₂O/0.16 NaOH/100 Ethanol. Following the hydrothermal reaction, the solid product was recovered, filtered, washed with deionized water until the pH of the washing water was neutral, dried at 120 °C overnight, and calcined in air at 823 K for 8 h to remove the TPAOH and structure directing agent, and obtain nano-ZSM-5.

The nano-ZSM-5 was then ion-exchanged in a 1 M solution of NH₄NO₃ (Merck) dissolved in water. The ion exchange took place under continuous stirring at 323 K for 2 h and was repeated three times to obtain nano-NH₄ZSM-5. The nano-NH₄ZSM-5 was calcined at 823 K for 4 h, with a temperature ramp of 1 K min⁻¹, which resulted in nano-HZSM-5 (n-HZSM-5).

For the nano-HZSM-5/ γ -Al₂O₃ (Hybrid-50/50) catalyst, the synthesis route was identical to the synthesis of n-HZSM-5, but γ -Al₂O₃ was added under continuous stirring 30 min prior to the hydrothermal reaction. The addition of γ -Al₂O₃ prior to the crystallization of HZSM-5 has also been reported in the work of He et al. [51], but their nano-HZSM-5 synthesis differs from the method reported in this work. The addition of γ -Al₂O₃ resulted in a synthesis mixture aimed at 50 mass% nano-HZSM-5 and 50 mass% γ -Al₂O₃. The introduction of γ -Al₂O₃ prior to the crystallization allows the in-situ formation of nano-HZSM-5 crystals on the γ -Al₂O₃ surface, see Figure S1 for a schematic representation of the synthesis route of Hybrid-50/50. The subsequent crystallization and ion-exchange procedures were identical as for the n-HZSM-5.

3.2. Catalyst Characterization

Catalyst particles within the 100–150 μ m range were prepared by pressing the catalyst powders, followed by sieving. X-ray diffraction (XRD, Diffractometer Kristalloflex D5000 with Cu K α radiation) was performed to identify the materials after synthesis. All powder diffraction patterns were collected for 2 θ between 5° and 70°, with a step of 0.02° and 30 s counting time for each angle. The mean crystal sizes were estimated by application of the Scherrer equation:

$$d = \frac{K\lambda}{\beta \cos\theta} \quad (1)$$

with d the mean crystal size (nm), K a dimensionless shape factor with a value of 1 [59], λ the wavelength of the X-rays, β the full-width at half-maximum (corrected for the instrumental error), and θ Bragg's angle.

The surface area and pore volume of the catalysts were determined by N₂-sorption at 77 K (Micromeritics Tristar). Before the measurements, the samples were degassed at 573 K for 4 h under a continuous N₂ flow. The BET-method was used to obtain the surface area S_{BET}, the t-plot method

for micropore area and micropore volume (V_{micro}), and the single-point adsorption for the total pore volume (V_t). The external surface area of the self-synthesized catalysts was determined by performing the N_2 -sorption prior to calcining the materials. To increase the accuracy of the S_{BET} of the materials containing micropores (HZSM-5, Hybrid-50/50, and the PM-50/50), Rouquerol's criteria were applied [60]. The pore size distribution (PSD) was determined by analyzing the adsorption branch of the isotherm, by applying the Barrett, Joyner, and Halenda (BJH) method for the mesoporous materials, and by a non-local density functional theory (NLDFIT) method, assuming cylindrical pore geometries for ZSM-5 [39,61]. The measurements of the c-HZSM-5 and n-HZSM-5 were initiated at low relative pressure.

NH_3 -TPD (Micromeritics Autochem) was used for the determination of the number of acid sites, assuming that each medium and strongly adsorbed NH_3 leads to one catalytically active acid site [62]. Then, 0.1 g catalyst was dried at 573 K under a continuous helium flow during 1 h to remove any surface-bound gases or moisture. Subsequently, the sample was saturated with NH_3 by flowing a 4 mol% NH_3/He flow for 1 h over the catalyst, and any unbound NH_3 molecules were flushed from the sample by helium at a temperature of 423 K. Desorption of NH_3 was achieved by increasing the temperature to 873 K at a rate of 10 K min^{-1} and was monitored using a thermal conductivity detector (TCD) and a mass spectrometer (MS), which were calibrated prior to every run. The obtained spectra were deconvoluted into three peaks, attributed to: Weak, medium, and strong acid sites. Integration of the peaks associated with the medium and strongly bound ammonia was assumed to result in the number of catalytically active acid sites (C_a) for each catalyst. To assess the strength of the bonding between the catalyst surface and the NH_3 , the NH_3 -desorption energy was determined through measuring the NH_3 -TPD profiles at different heating rates and then solving the Kissinger equation [63].

$$2\ln T_M - \ln \beta = \ln \frac{E_d}{R A_d} + \frac{E_d}{R} \frac{1}{T_M} \quad (2)$$

where T_M is the maximum desorption temperature of the highest temperature peak (typically around 673 K), β is the heating ramp (K min^{-1}), E_d the NH_3 -desorption energy (J mol^{-1}), R the universal gas constant ($\text{J mol}^{-1} \text{K}^{-1}$), and A_d the pre-exponential factor for the desorption. The calculated E_d does not take into account the amount of acid sites, but is solely dependent on the change in the peak position with the change in the heating ramp, similar to how activation energy is calculated.

Scanning electron microscopy (SEM, FEI Quanta 200F) was used to study the shape and size of the catalysts. Where XRD gives an average crystal size, SEM can give insights into the range of the crystal sizes. By SEM, it is also possible to qualitatively study the dispersion of the ZSM-5 crystals on the $\gamma\text{-Al}_2\text{O}_3$ surface for the Hybrid-50/50 catalyst and compare it to the PM-50/50.

Energy-dispersive X-ray spectroscopy (EDX) was used to determine the Si/Al ratio of the c-HZSM-5 and n-HZSM-5, where for c-HZSM-5, this was 28.1, close to the reported 25 by the manufacturer, and, for n-HZSM-5, the determined Si/Al ratio was 25.3, very close to the aimed ratio of 25. For Hybrid-50/50, we could not accurately determine the Si/Al ratio of the zeolite nanocrystals, due to the presence of $\gamma\text{-Al}_2\text{O}_3$ near the crystals.

3.3. Catalytic Testing

The catalytic experiments were performed on an identical setup as previous work [30,31,38]: The reactions were performed in a set of tubular reactors with a length of 0.85 m and an inner diameter of 0.0022 m. The catalyst was loaded in the reactor and diluted with inert α -alumina until 10 mass% of catalyst to avoid temperature deviations across the catalyst bed. The catalyst weight range was limited to between 0.005 and 0.2 g. Liquid n-butanol (Merck, >99.5%) was fed through a Coriolis mass flow controller. The inlet partial pressure of n-butanol in the reactors was regulated to 29 kPa by adding N_2 (Air Liquide) as a carrier gas. Prior to reaction, the reactors and catalyst bed were heated to the reaction temperature under a N_2 flow for 1 h, to ensure the complete reactor tubes were at reaction temperature and remained stable. All downstream lining was heated to 443 K to avoid

condensation. To achieve a working pressure of 5 bar, a back pressure regulator was used. Online analysis of the reactor effluent was performed with a GC-FID (with a 100 m PONA column), with CH₄ (Air Liquide) as an internal standard. The only detected species were n-butanol (the feed), dibutyl ether, butenes, and the internal standard. No other (oxygenated) hydrocarbons were detected; therefore, based on reaction stoichiometry, the amount of water being formed was calculated. The resulting material balance of the results shown in this work closed within 5%. To ensure intrinsic kinetics were measured, literature correlations were utilized [64]. The different acid site densities of each catalyst were compensated for by comparing the catalysts based on site time:

$$\text{site time} = \frac{W C_a}{F_{BuOH}^0} \quad (3)$$

with W (kg) the mass of the catalyst, C_a (mol kg⁻¹) the acid site density, and F_{BuOH}^0 (mol s⁻¹) the molar flow rate of n-butanol at the inlet.

The activity of the catalysts is based on the conversion of n-butanol (X_{BuOH}) and is defined as:

$$X_{BuOH} = \frac{F_{BuOH}^0 - F_{BuOH}}{F_{BuOH}^0} \quad (4)$$

where F_{BuOH} (mol s⁻¹) is the molar flow rate of n-butanol at the outlet of the reactor as determined by GC analysis. The activity can also be expressed as site time yield (STY, in s⁻¹):

$$\text{STY} = \frac{X_{BuOH}}{\tau} \quad (5)$$

The STY is similar to a turnover frequency but is averaged over the complete reactor. The carbon selectivity (S_i) toward the product is expressed as:

$$S_i = \frac{c_i F_i}{4(F_{BuOH}^0 - F_{BuOH})} \quad (6)$$

with F_i the outlet flow rate of product i , and c_i the number of carbon atoms per molecule of product i .

4. Conclusions

HZSM-5 and γ -Al₂O₃ are widely used materials in heterogeneous catalysis and they could be key materials to process bio-derived compounds. To attenuate their disadvantages and combine their advantages, a hybrid catalyst composed of nano-HZSM-5 crystals dispersed on a γ -Al₂O₃ surface was in-situ hydrothermally synthesized. The hybrid catalyst's performance for the dehydration of n-butanol was compared with commercially available HZSM-5 and γ -Al₂O₃, and with synthesized nano-HZSM-5 and a physical mixture of nano-HZSM-5 and γ -Al₂O₃.

Through characterization of the materials, it was found that for the hybrid catalyst, the nanozeolite crystals were dispersed on the alumina surface, while in the physical mixture, there were domains of HZSM-5 and domains of γ -Al₂O₃. The synthesis procedure led to a different acid strength distribution compared to nano-HZSM-5 and pristine γ -Al₂O₃, where there was a shift toward more mildly acidic sites. The commercially available HZSM-5 had irregular, aggregated crystals with a size ranging from 80 to 600 nm, whilst the synthesized nano-HZSM-5 had a hexagonal shape, with a small crystal size distribution of 80–180 nm. The activity of the commercially available HZSM-5 was the highest, related to its high amount of strong acid sites. The activity of the hybrid catalyst was higher than that of the physical mixture, and both were intermediate between HZSM-5 and γ -Al₂O₃.

The selectivity toward dibutyl ether at low conversion was the lowest for the hybrid catalyst, which was related to the synthesis procedure and, consequently, altered the strongest acid sites on γ -Al₂O₃, leading to a decrease in ether formation. The selectivity was significantly different from the

physical mixture, indicating an interaction between γ -Al₂O₃ and the nano-HZSM-5 crystals. The lower selectivity to dibutyl ether over the hybrid catalyst could explain the higher activity compared to the physical mixture.

The order of catalytic stability under n-butanol dehydration conditions was: γ -Al₂O₃ = the hybrid catalyst >> the physical mixture > nano-HZSM-5 > commercial HZSM-5. Whilst the hybrid catalyst was as stable as γ -Al₂O₃, it showed much higher selectivity toward butenes. In fact, the selectivity over the hybrid catalyst during the deactivation experiment was very similar to that of the nano-HZSM-5.

The combination of a relatively high activity, a high selectivity toward olefins, and very high stability indicate that the hybrid catalyst's performance benefits from the nano-HZSM-5 crystals being in the vicinity of γ -Al₂O₃ and being well-dispersed on it. The hybrid catalyst outperformed every tested material when aiming for long-term olefin production under mild conditions. Future work could focus on the finetuning of the acid strength and degree of micropores/mesopores through changing the ratio of nano-HZSM-5/ γ -Al₂O₃.

Supplementary Materials: The following are available online at <http://www.mdpi.com/2073-4344/10/8/879/s1>. Figure S1: Schematic representation of hybrid catalyst synthesis (SDA = structure directing agent, in our case tetrapropyl ammonium hydroxide, TEOS = tetraethyl orthosilicate), Figure S2. NH₃-TPD spectra for c-HZSM-5 (black), n-HZSM-5 (red), PM-50/50 (grey), Hybrid-50/50 (green) and γ -Al₂O₃ (blue). Starting temperature = 150 °C, heating ramp = 10 K min⁻¹, the intensities are weight-normalized, Figure S3. NH₃-TPD profiles with deconvolution of c-HZSM-5 (a), n-HZSM-5 (b), PM-50/50 (c), Hybrid-50/50 (d) and γ -Al₂O₃ (e). The weak acid site contribution to the spectrum is depicted as (—), the medium acid sites as (-.-) and the strong acid sites as (...), Figure S4. SEM-images of c-HZSM-5 (a) n-HZSM-5, with crystal size bars (b) and Hybrid-50/50 (c,d), Figure S5. Selectivity of products versus conversion, c-HZSM-5 (■, black), n-HZSM-5 (■, red), PM-50/50 (▲, purple), Hybrid-50/50 (◆, green) and γ -Al₂O₃ (●, blue). Temperature = 513 K, inlet pressure of n-butanol = 29 kPa, total pressure = 5 bar. Error bars indicate the 95% confidence interval.

Author Contributions: Conceptualization, A.d.R., M.K.S. and A.V.; methodology, A.d.R. and T.V.; formal analysis, A.d.R. and T.V.; investigation, A.d.R. and T.V.; data curation, A.d.R. and T.V.; writing—original draft preparation, A.d.R. and T.V.; writing—review and editing, A.d.R., T.V., M.K.S. and A.V.; supervision, M.K.S. and A.V. All authors have read and agreed to the published version of the manuscript.

Funding: This research received no external funding.

Acknowledgments: T.V. acknowledges financial support from a doctoral fellowship (1SA7520N) from the Research-Foundation Flanders (FWO).

Conflicts of Interest: The authors declare no conflict of interest.

References

- Baeyens, J.; Kang, Q.; Appels, L.; Dewil, R.; Lv, Y.Q.; Tan, T.W. Challenges and opportunities in improving the production of bio-ethanol. *Prog. Energy Combust. Sci.* **2015**, *47*, 60–88. [[CrossRef](#)]
- Ni, Y.; Sun, Z.H. Recent progress on industrial fermentative production of acetone-butanol-ethanol by *Clostridium acetobutylicum* in China. *Appl. Microbiol. Biotechnol.* **2009**, *83*, 415–423. [[CrossRef](#)] [[PubMed](#)]
- Lee, D.-H. Bio-based economies in Asia: Economic analysis of development of bio-based industry in China, India, Japan, Korea, Malaysia and Taiwan. *Int. J. Hydrog. Energy* **2016**, *41*, 4333–4346. [[CrossRef](#)]
- Waldron, K.W. *Bioalcohol Production: Biochemical Conversion of Lignocellulosic Biomass*; Elsevier: Amsterdam, The Netherlands, 2010.
- Weber, C.; Farwick, A.; Benisch, F.; Brat, D.; Dietz, H.; Subtil, T.; Boles, E. Trends and challenges in the microbial production of lignocellulosic bioalcohol fuels. *Appl. Microbiol. Biotechnol.* **2010**, *87*, 1303–1315. [[CrossRef](#)] [[PubMed](#)]
- Enguïdanos, M.; Soria, A.; Kavalov, B.; Jensen, P. Techno-economic analysis of bio-alcohol production in the eu: A short summary for decision-makers. *Eur. Comm. Rep. EUR* **2002**, 20280.
- Hergueta, C.; Tsolakis, A.; Herreros, J.M.; Bogarra, M.; Price, E.; Simmance, K.; York, A.P.E.; Thompson, D. Impact of bio-alcohol fuels combustion on particulate matter morphology from efficient gasoline direct injection engines. *Appl. Energy* **2018**, *230*, 794–802. [[CrossRef](#)]
- He, Z.; Yang, M.; Wang, X.; Zhao, Z.; Duan, A. Effect of the transition metal oxide supports on hydrogen production from bio-ethanol reforming. *Catal. Today* **2012**, *194*, 2–8. [[CrossRef](#)]

9. Shylesh, S.; Kim, D.; Ho, C.R.; Johnson, G.R.; Wu, J.; Bell, A.T. Non-Oxidative Dehydrogenation Pathways for the Conversion of C2–C4 Alcohols to Carbonyl Compounds. *ChemSusChem* **2015**, *8*, 3959–3962. [[CrossRef](#)]
10. Zimmermann, H. Propene. In *Ullmann's Encyclopedia of Industrial Chemistry*; Wiley-VCH Verlag GmbH & Co. KGaA: Weinheim, BW, Germany, 2013.
11. Zimmermann, H.; Walzl, R. Ethylene. In *Ullmann's Encyclopedia of Industrial Chemistry*; Wiley-VCH Verlag GmbH & Co. KGaA: Weinheim, BW, Germany, 2000.
12. Cundy, C.S.; Cox, P.A. The Hydrothermal Synthesis of Zeolites: History and Development from the Earliest Days to the Present Time. *Chem. Rev.* **2003**, *103*, 663–702. [[CrossRef](#)]
13. Jacobs, P.A.; Dusselier, M.; Sels, B.F. Will Zeolite-Based Catalysis be as Relevant in Future Biorefineries as in Crude Oil Refineries? *Angew. Chem. Int. Ed.* **2014**, *53*, 8621–8626. [[CrossRef](#)]
14. Kasztelan, S.; Payen, E.; Toulhoat, H.; Grimblot, J.; Bonnelle, J.P. Industrial MoO₃-promoter oxide- γ -Al₂O₃ hydrotreating catalysts: Genesis and architecture description. *Polyhedron* **1986**, *5*, 157–167. [[CrossRef](#)]
15. Wang, J.; Dong, L.; Hu, Y.; Zheng, G.; Hu, Z.; Chen, Y. Dispersion of NiO supported on γ -Al₂O₃ and TiO₂/ γ -Al₂O₃ supports. *J. Solid State Chem.* **2001**, *157*, 274–282. [[CrossRef](#)]
16. Akah, A.; Al-Ghrami, M. Maximizing propylene production via FCC technology. *Appl. Petrochem. Res.* **2015**, *5*, 377–392. [[CrossRef](#)]
17. Adewuyi, Y.G.; Klocke, D.J.; Buchanan, J.S. Effects of high-level additions of ZSM-5 to a fluid catalytic cracking (FCC) RE-USY catalyst. *Appl. Catal. A Gen.* **1995**, *131*, 121–133. [[CrossRef](#)]
18. Hu, H.; Lyu, J.; Rui, J.; Cen, J.; Zhang, Q.; Wang, Q.; Han, W.; Li, X. The effect of Si/Al ratio on the catalytic performance of hierarchical porous ZSM-5 for catalyzing benzene alkylation with methanol. *Catal. Sci. Technol.* **2016**, *6*, 2647–2652. [[CrossRef](#)]
19. Odedairo, T.; Balasamy, R.J.; Al-Khattaf, S. Influence of mesoporous materials containing ZSM-5 on alkylation and cracking reactions. *J. Mol. Catal. A Chem.* **2011**, *345*, 21–36. [[CrossRef](#)]
20. Weckhuysen, B.M.; Yu, J. Recent advances in zeolite chemistry and catalysis. *Chem. Soc. Rev.* **2015**, *44*, 7022–7024. [[CrossRef](#)]
21. Müller, S.; Liu, Y.; Vishnuvarthan, M.; Sun, X.; van Veen, A.C.; Haller, G.L.; Sanchez-Sanchez, M.; Lercher, J.A. Coke formation and deactivation pathways on H-ZSM-5 in the conversion of methanol to olefins. *J. Catal.* **2015**, *325*, 48–59. [[CrossRef](#)]
22. Sheng, Q.; Ling, K.; Li, Z.; Zhao, L. Effect of steam treatment on catalytic performance of HZSM-5 catalyst for ethanol dehydration to ethylene. *Fuel Process. Technol.* **2013**, *110*, 73–78. [[CrossRef](#)]
23. Ji, Y.; Yang, H.; Yan, W. Strategies to Enhance the Catalytic Performance of ZSM-5 Zeolite in Hydrocarbon Cracking: A Review. *Catalysts* **2017**, *7*, 367. [[CrossRef](#)]
24. Ni, M.; Leung, D.Y.C.; Leung, M.K.H. A review on reforming bio-ethanol for hydrogen production. *Int. J. Hydrog. Energy* **2007**, *32*, 3238–3247. [[CrossRef](#)]
25. Euzen, P.; Raybaud, P.; Krokidis, X.; Toulhoat, H.; Le Loarer, J.-L.; Jolivet, J.-P.; Froidefond, C. Alumina. In *Handbook of Porous Solids*; Wiley-VCH Verlag GmbH & Co. KGaA: Weinheim, BW, Germany, 2008.
26. Coulier, L.; Kishan, G.; van Veen, J.A.R.; Niemantsverdriet, J.W. Influence of Support-Interaction on the Sulfidation Behavior and Hydrodesulfurization Activity of Al₂O₃-Supported W, CoW, and NiW Model Catalysts. *J. Phys. Chem. B* **2002**, *106*, 5897–5906. [[CrossRef](#)]
27. López Cordero, R.; López Agudo, A. Effect of water extraction on the surface properties of Mo/Al₂O₃ and NiMo/Al₂O₃ hydrotreating catalysts. *Appl. Catal. A Gen.* **2000**, *202*, 23–35. [[CrossRef](#)]
28. Samain, L.; Jaworski, A.; Edén, M.; Ladd, D.M.; Seo, D.-K.; Javier Garcia-Garcia, F.; Häussermann, U. Structural analysis of highly porous γ -Al₂O₃. *J. Solid State Chem.* **2014**, *217*, 1–8. [[CrossRef](#)]
29. Ghamsari, M.S.; Mahzar, Z.A.S.; Radiman, S.; Hamid, A.M.A.; Khalilabad, S.R. Facile route for preparation of highly crystalline γ -Al₂O₃ nanopowder. *Mater. Lett.* **2012**, *72*, 32–35. [[CrossRef](#)]
30. Gunst, D.; Alexopoulos, K.; Van Der Borght, K.; John, M.; Galvita, V.; Reyniers, M.-F.; Verberckmoes, A. Study of butanol conversion to butenes over H-ZSM-5: Effect of chemical structure on activity, selectivity and reaction pathways. *Appl. Catal. A Gen.* **2017**, *539*, 1–12. [[CrossRef](#)]
31. Gunst, D.; Sabbe, M.; Reyniers, M.-F.; Verberckmoes, A. Study of n-butanol conversion to butenes: Effect of Si/Al ratio on activity, selectivity and kinetics. *Appl. Catal. A Gen.* **2019**, *582*, 117101. [[CrossRef](#)]
32. Fan, D.; Dai, D.J.; Wu, H.S. Ethylene Formation by Catalytic Dehydration of Ethanol with Industrial Considerations. *Materials* **2013**, *6*, 101–115. [[CrossRef](#)]

33. Kang, M.; DeWilde, J.F.; Bhan, A. Kinetics and Mechanism of Alcohol Dehydration on γ -Al₂O₃: Effects of Carbon Chain Length and Substitution. *ACS Catal.* **2015**, *5*, 602–612. [[CrossRef](#)]
34. Roy, S.; Mpourmpakis, G.; Hong, D.Y.; Vlachos, D.G.; Bhan, A.; Gorte, R.J. Mechanistic Study of Alcohol Dehydration on γ -Al₂O₃. *ACS Catal.* **2012**, *2*, 1846–1853. [[CrossRef](#)]
35. Chiang, H.; Bhan, A. Catalytic consequences of hydroxyl group location on the rate and mechanism of parallel dehydration reactions of ethanol over acidic zeolites. *J. Catal.* **2010**, *271*, 251–261. [[CrossRef](#)]
36. Yakovleva, I.S.; Banzaraksaeva, S.P.; Ovchinnikova, E.V.; Chumachenko, V.A.; Isupova, L.A. Catalytic Dehydration of Bioethanol to Ethylene. *Catal. Ind.* **2016**, *8*, 152–167. [[CrossRef](#)]
37. Zhang, M.H.; Yu, Y.Z. Dehydration of Ethanol to Ethylene. *Ind. Eng. Chem. Res.* **2013**, *52*, 9505–9514. [[CrossRef](#)]
38. de Reviere, A.; Gunst, D.; Sabbe, M.; Verberckmoes, A. Sustainable short-chain olefin production through simultaneous dehydration of mixtures of 1-butanol and ethanol over HZSM-5 and γ -Al₂O₃. *J. Ind. Eng. Chem.* **2020**, *89*, 257–272. [[CrossRef](#)]
39. Al-Dughaiter, A.S.; de Lasa, H. HZSM-5 zeolites with different SiO₂/Al₂O₃ ratios. Characterization and NH₃ desorption kinetics. *Ind. Eng. Chem. Res.* **2014**, *53*, 15303–15316. [[CrossRef](#)]
40. Trueba, M.; Trasatti, S.P. Γ -alumina as a support for catalysts: A review of fundamental aspects. *Eur. J. Inorg. Chem.* **2005**, *2005*, 3393–3403. [[CrossRef](#)]
41. Shao, J.; Fu, T.; Ma, Q.; Ma, Z.; Zhang, C.; Li, Z. Controllable synthesis of nano-ZSM-5 catalysts with large amount and high strength of acid sites for conversion of methanol to hydrocarbons. *Microporous Mesoporous Mater.* **2019**, *273*, 122–132. [[CrossRef](#)]
42. Qureshi, B.A.; Lan, X.; Arslan, M.T.; Wang, T. Highly Active and Selective Nano H-ZSM-5 Catalyst with Short Channels along b-axis for Glycerol Dehydration to Acrolein. *Ind. Eng. Chem. Res.* **2019**, *58*, 12611–12622. [[CrossRef](#)]
43. Fu, T.; Chang, J.; Shao, J.; Li, Z. Fabrication of a nano-sized ZSM-5 zeolite with intercrystalline mesopores for conversion of methanol to gasoline. *J. Energy Chem.* **2017**, *26*, 139–146. [[CrossRef](#)]
44. Huangfu, J.J.; Mao, D.S.; Zhai, X.L.; Guo, Q.S. Remarkably enhanced stability of HZSM-5 zeolite co-modified with alkaline and phosphorous for the selective conversion of bio-ethanol to propylene. *Appl. Catal. A Gen.* **2016**, *520*, 99–104. [[CrossRef](#)]
45. Takahashi, A.; Xia, W.; Nakamura, I.; Shimada, H.; Fujitani, T. Effects of added phosphorus on conversion of ethanol to propylene over ZSM-5 catalysts. *Appl. Catal. A Gen.* **2012**, *423–424*, 162–167. [[CrossRef](#)]
46. Stein, A. Advances in Microporous and Mesoporous Solids—Highlights of Recent Progress. *Adv. Mater.* **2003**, *15*, 763–775. [[CrossRef](#)]
47. Karlsson, A.; Stöcker, M.; Schäfer, K. In situ Synthesis of Micro- and Mesoporous Al-MFI/MCM-41 like Phases with High Hydrothermal Stability. In *Studies in Surface Science and Catalysis*; Sayari, A., Jaroniec, M., Eds.; Elsevier: Amsterdam, The Netherlands, 2000; Volume 129, pp. 99–106.
48. Habib, S.; Launay, F.; Laforge, S.; Comparot, J.-D.; Faust, A.-C.; Millot, Y.; Onfroy, T.; Montouillout, V.; Magnoux, P.; Paillaud, J.-L.; et al. High catalytic cracking activity of Al-MCM-41 type materials prepared from ZSM-5 zeolite crystals and fumed silica. *Appl. Catal. A Gen.* **2008**, *344*, 61–69. [[CrossRef](#)]
49. Chen, G.W.; Li, S.L.; Jiao, F.J.; Yuan, Q. Catalytic dehydration of bioethanol to ethylene over TiO₂/ γ -Al₂O₃ catalysts in microchannel reactors. *Catal. Today* **2007**, *125*, 111–119. [[CrossRef](#)]
50. Wu, J.; Liu, H.-J.; Yan, X.; Zhou, Y.-J.; Lin, Z.-N.; Mi, S.; Cheng, K.-K.; Zhang, J.-A. Efficient Catalytic Dehydration of High-Concentration 1-butanol with Zn-Mn-Co modified γ -Al₂O₃ in Jet Fuel Production. *Catalysts* **2019**, *9*, 93. [[CrossRef](#)]
51. He, Z.; Jiao, Q.; Fang, Z.; Li, T.; Feng, C.; Li, H.; Zhao, Y. Light olefin production from catalytic pyrolysis of waste tires using nano-HZSM-5/ γ -Al₂O₃ catalysts. *J. Anal. Appl. Pyrolysis* **2018**, *129*, 66–71. [[CrossRef](#)]
52. Qin, Z.; Pinard, L.; Benghalem, M.A.; Daou, T.J.; Melinte, G.; Ersen, O.; Asahina, S.; Gilson, J.-P.; Valtchev, V. Preparation of Single-Crystal “House-of-Cards”-like ZSM-5 and Their Performance in Ethanol-to-Hydrocarbon Conversion. *Chem. Mater.* **2019**, *31*, 4639–4648. [[CrossRef](#)]
53. van Steen, E.; Claeys, I.M.; Callanan, L.H. (Eds.) Recent Advances in the Science and Technology of Zeolites and Related materials. In *Studies in Surface Science and Catalysis*; Elsevier: Amsterdam, The Netherlands, 2004; Volume 154.
54. Huang, S.; Zhao, Z.; Chen, X.; Li, F. Alkali extraction of valuable metals from spent Mo-Ni/Al₂O₃ catalyst. *Int. J. Refract. Met. Hard Mater.* **2014**, *46*, 109–116. [[CrossRef](#)]

55. Eder, F.; Stockenhuber, M.; Lercher, J.A. Brønsted Acid Site and Pore Controlled Siting of Alkane Sorption in Acidic Molecular Sieves. *J. Phys. Chem. B* **1997**, *101*, 5414–5419. [[CrossRef](#)]
56. Wang, Z.; O'Dell, L.A.; Zeng, X.; Liu, C.; Zhao, S.; Zhang, W.; Gaborieau, M.; Jiang, Y.; Huang, J. Insight into Three-Coordinate Aluminum Species on Ethanol-to-Olefin Conversion over ZSM-5 Zeolites. *Angew. Chem. Int. Ed.* **2019**, *58*, 18061–18068. [[CrossRef](#)]
57. Larmier, K.; Chizallet, C.; Cadran, N.; Maury, S.; Abboud, J.; Lamic-Humblot, A.-F.; Marceau, E.; Lauron-Pernot, H. Mechanistic Investigation of Isopropanol Conversion on Alumina Catalysts: Location of Active Sites for Alkene/Ether Production. *ACS Catal.* **2015**, *5*, 4423–4437. [[CrossRef](#)]
58. Castaño, P.; Ruiz-Martínez, J.; Epelde, E.; Gayubo, A.G.; Weckhuysen, B.M. Spatial Distribution of Zeolite ZSM-5 within Catalyst Bodies Affects Selectivity and Stability of Methanol-to-Hydrocarbons Conversion. *ChemCatChem* **2013**, *5*, 2827–2831. [[CrossRef](#)]
59. Song, W.; Justice, R.E.; Jones, C.A.; Grassian, V.H.; Larsen, S.C. Synthesis, Characterization, and Adsorption Properties of Nanocrystalline ZSM-5. *Langmuir* **2004**, *20*, 8301–8306. [[CrossRef](#)] [[PubMed](#)]
60. Rouquerol, J.; Llewellyn, P.; Rouquerol, F. Is the BET equation applicable to microporous adsorbents? In *Studies in Surface Science and Catalysis*; Llewellyn, P.L., Rodriguez-Reinoso, F., Rouquerol, J., Seaton, N., Eds.; Elsevier: Amsterdam, The Netherlands, 2007; Volume 160, pp. 49–56.
61. Groen, J.C.; Peffer, L.A.A.; Pérez-Ramírez, J. Pore size determination in modified micro- and mesoporous materials. Pitfalls and limitations in gas adsorption data analysis. *Microporous Mesoporous Mater.* **2003**, *60*, 1–17. [[CrossRef](#)]
62. Van der Borgh, K.; Galvita, V.V.; Marin, G.B. Ethanol to higher hydrocarbons over Ni, Ga, Fe-modified ZSM-5: Effect of metal content. *Appl. Catal. A Gen.* **2015**, *492*, 117–126. [[CrossRef](#)]
63. Kissinger, H.E. Variation of Peak Temperature with Heating Rate in Differential Thermal Analysis. *J. Res. Natl. Bur. Stand.* **1956**, *57*, 217–221. [[CrossRef](#)]
64. Berger, R.J.; Stitt, E.H.; Marin, G.B.; Kapteijn, F.; Moulijn, J.A. Eurokin-Chemical Reaction Kinetics in Practice. *Cattech* **2001**, *5*, 30–60. [[CrossRef](#)]



© 2020 by the authors. Licensee MDPI, Basel, Switzerland. This article is an open access article distributed under the terms and conditions of the Creative Commons Attribution (CC BY) license (<http://creativecommons.org/licenses/by/4.0/>).